
Microwave Absorption Potential of $\text{La}_{0.7}[\text{X}_{0.95}\text{Y}_{0.05}]_{0.3}\text{MnO}_3$ with Dual-Doped Sites {XY = (Ca,Ba), (Ca,Sr), and (Sr,Ba)}

Apriatin¹, Siti Ahmiatri Saptari^{1*}, Arif Tjahjono¹, Hadiyawarman²

¹Departemen of Physics, Universitas Islam Negeri Syarif Hidayatullah Jakarta, Indonesia

²Research Center for Advanced Materials, National Research and Innovation Agency, Indonesia

sitti.ahmiatri@uinjkt.ac.id

Submitted: October; Revised: October; Approved: November; Available Online: December

Abstract. The technology in the field of electronic devices is currently advancing in line with the increasing usage by humans. This continuous and growing usage also increases the amount of microwave radiation generated. This leads to wave interference that can disrupt the functionality of application devices. Absorbing materials are a type of material that functions as a microwave absorber. This study engineered lanthanum manganate material, specifically $\text{La}_{0.7}[\text{X}_{0.95}\text{Y}_{0.05}]_{0.3}\text{MnO}_3$ {XY = (Ca,Ba), (Ca,Sr), and (Sr,Ba)}, synthesized using the sol-gel method. The X-Ray Diffraction characterization results showed that each sample has a single-phase orthorhombic structure with a space group of Pbnm (62). The Scanning Electron Microscope–Energy Dispersive Spectroscopy characterization revealed particle morphology with varying particle size distributions on a micro-scale. Based on Vibrating Sample Magnetometer results, the samples $\text{La}_{0.7}[\text{Ca}_{0.95}\text{Ba}_{0.05}]_{0.3}\text{MnO}_3$ and $\text{La}_{0.7}[\text{Ca}_{0.95}\text{Sr}_{0.05}]_{0.3}\text{MnO}_3$ exhibit paramagnetic properties, while $\text{La}_{0.7}[\text{Sr}_{0.95}\text{Ba}_{0.05}]_{0.3}\text{MnO}_3$ exhibits superparamagnetic properties. Through Vector Network Analyzer characterization, it was found that lanthanum manganate doped with Ca, Ba, and Sr demonstrated high electromagnetic wave absorption capabilities, achieving an absorption rate of 97%–98% at frequencies of 10–10.5 GHz. Thus, $\text{La}_{0.7}[\text{X}_{0.95}\text{Y}_{0.05}]_{0.3}\text{MnO}_3$ {XY = (Ca,Ba), (Ca,Sr), and (Sr,Ba)} is a potential candidate as a microwave-absorbing material.

Keywords: $\text{La}_{0.7}[\text{X}_{0.95}\text{Y}_{0.05}]_{0.3}\text{MnO}_3$ {XY = (Ca,Ba), (Ca,Sr), and (Sr,Ba)}, microwave absorber, sol-gel

DOI : [10.15408/fiziya.v7i2.47935](https://doi.org/10.15408/fiziya.v7i2.47935)

©2022 The Author (s) This is an Open-access article under CC-BY-SA license
(<https://creativecommons.org/licenses/by-sa/4.0/>)

Al-Fiziya: Journal of Materials Science, Geophysics,
Instrumentation and Theoretical Physics
P-ISSN: 2621-0215, E-ISSN: 2621-489X

INTRODUCTION

In recent years, technology has shown rapid advancements, supporting progress in nearly every field, such as radar systems, communication networks, automotive tools, medical applications, and other applications utilizing electromagnetic waves [1]. Continuous use of devices can lead to electromagnetic radiation hazards, causing electromagnetic wave interference that may damage the functional components of these devices [2]. Microwave-absorbing materials play a crucial role in mitigating electromagnetic radiation in various applications [3]. Material engineering is employed as an effort to reduce negative impacts by developing materials capable of attenuating and absorbing electromagnetic waves by converting electromagnetic energy into other forms of energy as needed [4]. The mechanism of microwave absorption in a material involves interactions between the waves and the material, resulting in a reflection known as reflection loss (RL) [5], [6]. A material is considered a high-performance microwave absorber if it can absorb waves within a broad effective absorption bandwidth (EAB), covering frequency ranges where the reflection loss (RL) is below -10 dB, is lightweight, has good thermal stability, and can be tailored to the desired frequency bands for microwave absorption [7].

Perovskite oxides with the ABO_3 structure have gained significant interest due to their distinctive characteristics, including high structural stability, low density, heat resistance, and excellent electromagnetic properties [8], [9]. To date, studies on the crystal structure and electromagnetic properties of perovskites have demonstrated their potential for microwave absorption [10]. $LaMnO_3$ is a perovskite material with an ABO_3 structure belonging to the Pm-3m space group. La occupies the A-site, while Mn occupies the B-site at the center of the octahedral framework, coordinated with six oxygen ions [11], [12]. Lanthanum manganate ($LaMnO_3$) has become one of the most extensively developed materials due to properties that support wave absorption. Doping at the La site can influence the permittivity and magnetic properties, as indicated by the double exchange phenomenon [13]. This phenomenon arises when doping at the La site changes the Mn valence state to Mn^{3+} and Mn^{4+} , affecting the material's response to an external magnetic field [14].

Other studies report that doping with Sr^{2+} and Sm^{2+} impacts both dynamic and static magnetic properties [10]. The addition of Sr^{2+} and Sm^{2+} enhances the natural resonance and exchange resonance of the $LaMnO_3$ matrix, thereby improving microwave absorption performance [15]. In addition to $LaMnO_3$, $CaMnO_3$ is another promising material due to its wide perovskite structure, high thermal stability, and excellent thermoelectric properties [9], [16]. $CaMnO_3$, as a dielectric material, demonstrates microwave absorption mechanisms that are unaffected by the Curie temperature. Therefore, researchers suggest that this material also holds significant potential as a microwave-absorbing material [15].

Other perovskite materials such as LSM or lanthanum manganite doped with strontium are also widely researched materials because they have distinctive electronic and magnetic properties that can be applied to various technological applications [17], [18]. LSM has properties such as colossal magnetoresistance and magnetocaloric effect so that it is ferromagnetic at room temperature [19]. However, LSM material has one disadvantage, namely poor ionic conductivity [20], so it needs to be combined with other elements to find the right combination.

Research on the material $(La_{0.8}Ba_{0.2})(Mn_{0.4}Zn_{0.2}Fe_{0.4})O_3$ with $x = 0.2$ obtained X-ray diffraction pattern refinement results show that the sample has a single phase. The absorption of electromagnetic waves in the frequency range of 8-12 GHz was obtained at 96%, making it a potential candidate to be applied as an electromagnetic wave absorbing material [13]. $La_{0.7}Ca_{0.3}Mn_{1-x}Ti_xO_3$ which was studied using the sol-gel method, obtained VNA results that the sample with a concentration of $x = 0.3$ had the highest absorption ability reaching 90.16% and a value of -10.07202 dB at its optimal frequency of 10.4 GHz [21]. Ratna Isnanita Admi et al investigated $La_{0.7}(Ca_{1-x}Sr_x)_{0.3}MnO_3$ ($x = 0; 0.1; 0.2; \text{ and } 0.3$) samples synthesized using the sol-gel method. It shows that there is an increase in particle grain size due to the addition of Sr^{2+} . Microwave absorbing properties in the frequency range of 8-12 GHz are shown through an optimal absorption peak of about -3.53 dB for the $x = 0$ sample with a thickness of 1.5 mm [22].

In this study, we synthesized $La_{0.7}[X_{0.95}Y_{0.05}]_{0.3}MnO_3$ {XY = (Ca,Ba), (Ca,Sr), and (Sr,Ba)} using sol-gel method to analyze the phases formed, crystal system, morphology and particle size, magnetic properties, and microwave absorption properties. We also studied the effect of dopant addition to lanthanum manganate at La site on its absorbing ability.

EXPERIMENTAL SECTION

Materials

$La_{0.7}[X_{0.95}Y_{0.05}]_{0.3}MnO_3$ {XY = (Ca,Ba), (Ca,Sr), and (Sr,Ba)} samples were synthesized by sol-gel method. The materials used in this study include La_2O_3 (Merck, 99,99%), $Mn(NO_3)_2 \cdot 4H_2O$ (Merck, 98,5%), $Ca(NO_3)_2 \cdot 4H_2O$ (Merck, 99%), $Sr(NO_3)_2$ (Merck, 99%), $Ba(NO_3)_2$ (Merck, 99%), $C_6H_8O_7 \cdot H_2O$ (Merck, 99,5%), Nitric acid (HNO_3), 25% ammonia solution, distilled water, and 70% alcohol.

Methods

All materials were weighed first according to the stoichiometric ratio, then each material was dissolved with distilled water, especially La_2O_3 was dissolved using nitric acid (HNO_3) to become homogeneous with other nitrate-based precursors. Afterward, all solutions were mixed based on the samples to be made, namely $La_{0.7}[Ca_{0.95}Ba_{0.05}]_{0.3}MnO_3$, $La_{0.7}[Ca_{0.95}Sr_{0.05}]_{0.3}MnO_3$, and $La_{0.7}[Sr_{0.95}Ba_{0.05}]_{0.3}MnO_3$. The mixing of the solution was carried out in a fume hood using a hot plate that was heated while stirring until the solution reached a temperature of $+70^\circ C$, ammonia was added to obtain a solution pH of 7 and became a gel.

The samples that have become gels are then put into an oven at $200^\circ C$ for ± 3 hours with the aim of removing the water content in the sample so that the sample becomes a dry gel. Next, the calcination process is carried out in a furnace with heat up to $600^\circ C$ for 6 hours to remove the remaining organic compounds that may still remain. After that, it was continued with higher temperature heating to strengthen bonds and crystal formation, namely sintering at $1200^\circ C$ for 6 hours.

A series of sample processing processes were then followed by a characterization process consisting of X-ray diffraction (XRD) using Cu-K α radiation (1.5 Å) and scanned in the 2 θ range from angles of 3° to 90° with an increase of 0.02°, this test was carried out to determine the crystal parameters and phases formed from the sample. The morphology, grain size, alloy composition of the samples was examined using Scanning Electron Microscopy - Energy Dispersion Spectroscopy (SEM-EDS) with an accelerating voltage of 20 kV and magnification up to 20,000 times. The magnetic properties of the material were measured using a Vibrating Sample Magnetometer (VSM) with a magnetic field between 0 and 20,000 Oe at a temperature of 297 K. Then, the final test to determine the absorption value of the sample against microwaves through reflection loss (RL) using a Vector Network Analyzer whose measurement specifications are in the frequency range of 8-12 GHz with a gradual increase of 0.02 GHz.

RESULT AND DISCUSSION

Crystal Structure

La_{0.7}[X_{0.95}Y_{0.05}]_{0.3}MnO₃ {XY = (Ca,Ba), (Ca,Sr), dan (Sr,Ba)} material has been synthesized using sol gel method in the form of La_{0.7}Ca_{0.285}Ba_{0.015}MnO₃, La_{0.7}Ca_{0.285}Sr_{0.015}MnO₃, and La_{0.7}Sr_{0.285}Ba_{0.015}MnO₃. samples. The samples were characterized using XRD by producing diffraction patterns showing the phase of each sample as seen in Figure 1.

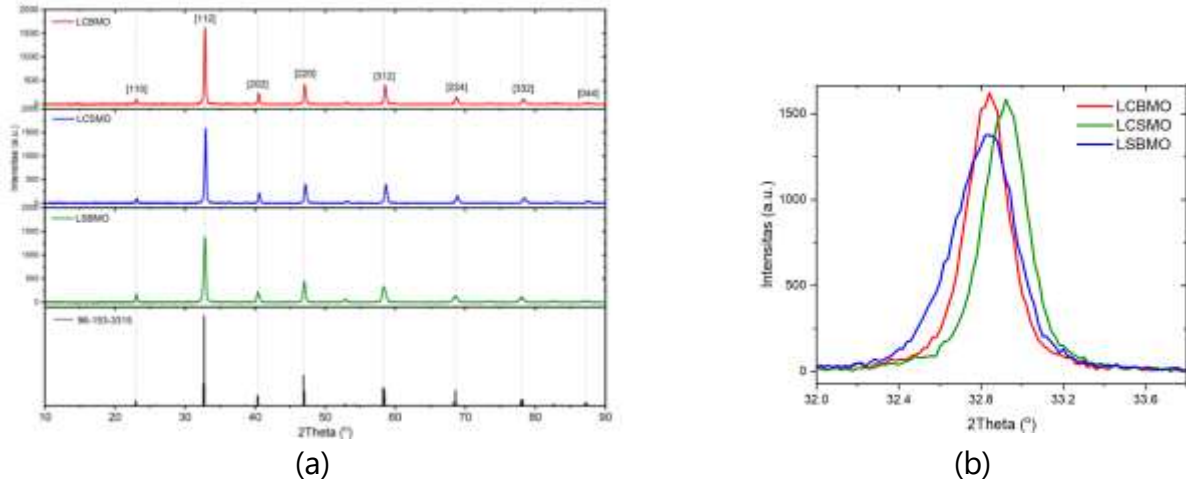


Figure 1. (a) XRD pattern of dari La_{0.7}[X_{0.95}Y_{0.05}]_{0.3}MnO₃ {XY = (Ca,Ba), (Ca,Sr), and (Sr,Ba)}, (b)

Diffraction pattern of the sample at the highest intensity.

In the figure, it can be seen that each sample has a single phase without any impurities. Figure 1 (b) shows a shift of the highest peak (at 112 hkl) by the LSBMO sample to a smaller angular position and a reduced intensity. This is because the substitution of Sr²⁺ and Ba²⁺ in La³⁺ causes a change in the lattice parameters to be larger [23]. This result is in accordance with Bragg's law which states that a small value will be produced if the distance between crystal planes is large. Bragg's law is written in equation (1) as follows:

$$2 d \sin \theta = n \lambda$$

(1)

d is the distance between planes, θ is the diffraction angle, n is the diffraction order (integer), and λ is the wavelength of the x-ray used [24], [25].

The results of XRD characterization in the form of diffractograms with the relationship between the angle 2θ and intensity are then processed quantitatively. The processing uses the Rietveld smoothing method with fit parameters that must be met based on the goodness of fit value $\chi^2 \leq 1.3$ [26] to obtain the structural parameters of each sample as presented in Table 1.

Table 1. Structural parameters of $\text{La}_{0.7}[\text{X}_{0.95}\text{Y}_{0.05}]_{0.3}\text{MnO}_3$ {XY = (Ca,Ba), (Ca,Sr), and (Sr,Ba)}

| Parameters | | LCBMO | LCSMO | LSBMO |
|---------------------------------|------------|---------|--------------|---------|
| Space Group | | | P b n m (62) | |
| Lattice Paramaters (Å) | a | 5.4709 | 5.4709 | 5.5120 |
| | b | 5.4597 | 5.4544 | 5.4679 |
| | c | 7.7152 | 7.7072 | 7.7481 |
| Volume (Å ³) | | 230.45 | 229.99 | 233.52 |
| Density (gram/cm ³) | | 6.158 | 6.149 | 6.332 |
| D_{W-H} (nm) | | 51.7794 | 47.2002 | 40.5756 |
| ε (%) | | 0.085 | 0.068 | 0.053 |
| D_{Mn-O} (Å) | D_a | 1.994 | 1.9932 | 2.0039 |
| | D_b | 1.917 | 1.916 | 1.9248 |
| | D_c | 1.9508 | 1.9489 | 1.9593 |
| $\theta_{Mn-O-Mn}$ | θ_a | 162.307 | 162.314 | 162.31 |
| | θ_b | 162.307 | 162.314 | 162.31 |
| | θ_c | 162.761 | 162.745 | 162.715 |
| W (%) | | 9.4784 | 9.4988 | 9.3303 |
| χ^2 | | 0.9237 | 0.9221 | 0.9993 |

Based on Table 1 above, it is shown that the three samples have an orthorhombic crystal system with space group Pbnm (62). The smallest average crystal size is owned by the LSBMO sample which is influenced by an increase in the lattice parameter. The crystal size was measured using the Williamson-Hall method with the strain of each sample less than 0.1. The Williamson-Hall method [27] is written as in Equation (2).

$$\beta \cos(\theta) = \frac{K\lambda}{D} + 4\varepsilon \sin(\theta)$$

(2)

where β is FWHM, K is constant (0.9), λ is the wavelength of the X-rays used (1.5406 Å), 4ε is a straightline equation with gradient m .

The Williamson-Hall method shows a linear relationship between $\text{FWHM} \cdot \cos(\theta)$ and $\sin(\theta)$ and then a graph of the relationship between $y = \text{FWHM} \cdot \cos(\theta)$ and $x = \sin(\theta)$ is obtained through the Least Squares Fit to Straight line approach [27] as shown in Figure 2 (a).

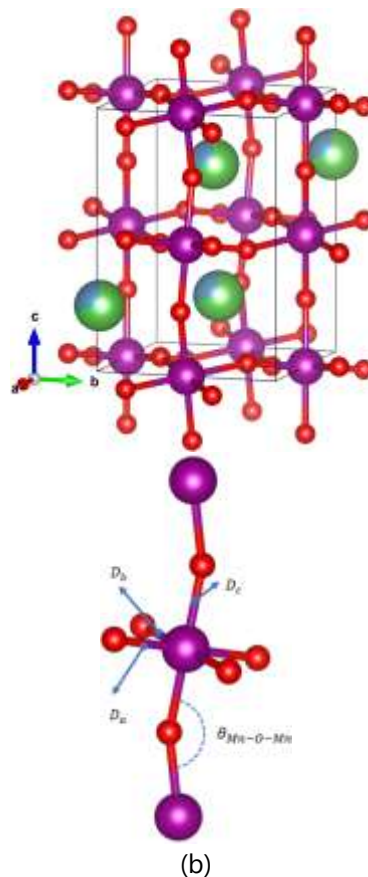
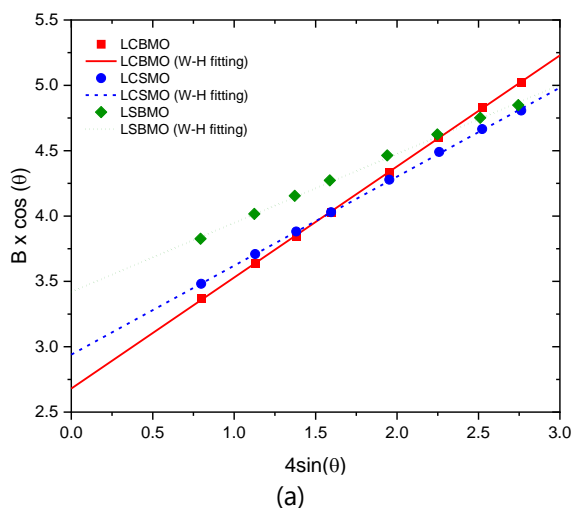


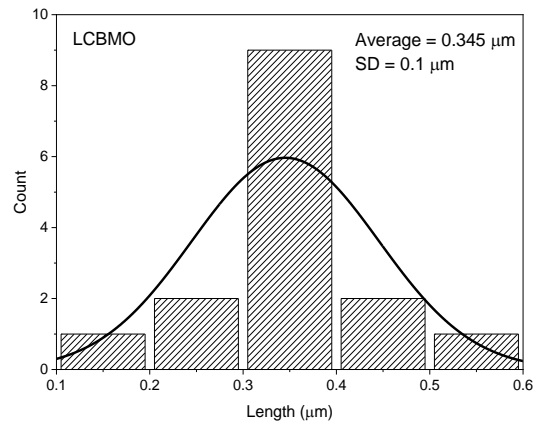
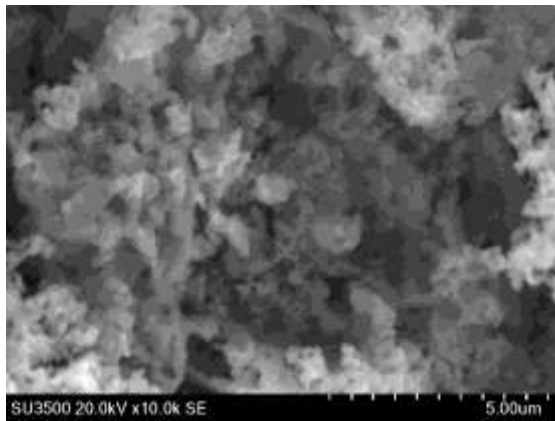
Figure 2. (a) Williamson-Hall plot, (b) The rhombohedral crystal system $\text{La}_{0.7}[\text{X}_{0.95}\text{Y}_{0.05}]_{0.3}\text{MnO}_3$ {XY = (Ca,Ba), (Ca,Sr), and (Sr,Ba)}

The rhombohedral crystal system in the sample is visualized as in Figure 2(b). The $\text{La}_{0.7}[\text{X}_{0.95}\text{Y}_{0.05}]_{0.3}\text{MnO}_3$ {XY = (Ca,Ba), (Ca,Sr), and (Sr,Ba)} material is known to experience a double exchange mechanism caused by the substitution of divalent ions for trivalent ions, in this case the La^{3+} oleh Ca^{2+} , Ba^{2+} , dan Sr^{2+} . This mechanism causes changes in Mn ions to Mn^{3+} dan Mn^{4+} which affect the material's response to magnetic fields. The double exchange mechanism is also influenced by the Mn-O bond length factor [22], [28]. The average bond length (Mn-O) and bond angle ($\angle \text{Mn-O-Mn}$) of each sample are LCBMO 1.954 (Å) and 162.458, LCSMO 1.953 (Å) and 162.458, and LSBMO 1.963 (Å) and 162.445, respectively.

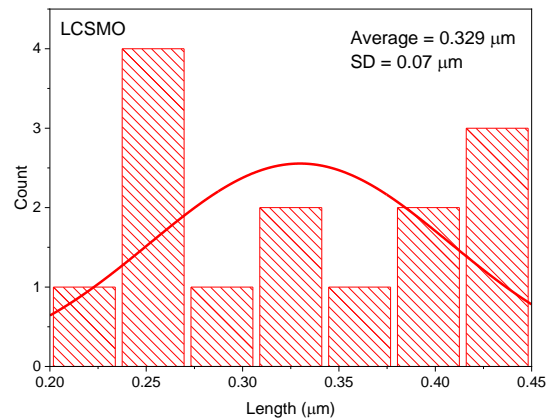
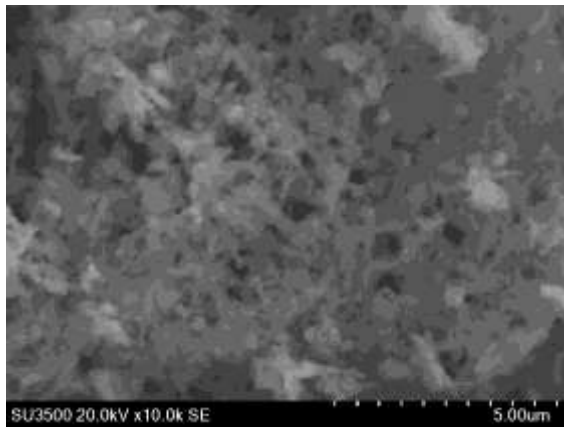
Morphology

SEM-EDS characterization results show the morphology and particle size distribution tested using magnification up to 20,000x with an accelerating voltage of 20kV. It can be seen that the three samples are homogeneous and the particles are distributed in micrometer size or the samples are microparticle materials. The average particle size of our samples is represented by measuring 15 grains obtained by ImageJ software measurements resulting in an image as presented in Figure 3.

(a)



(b)



(c)

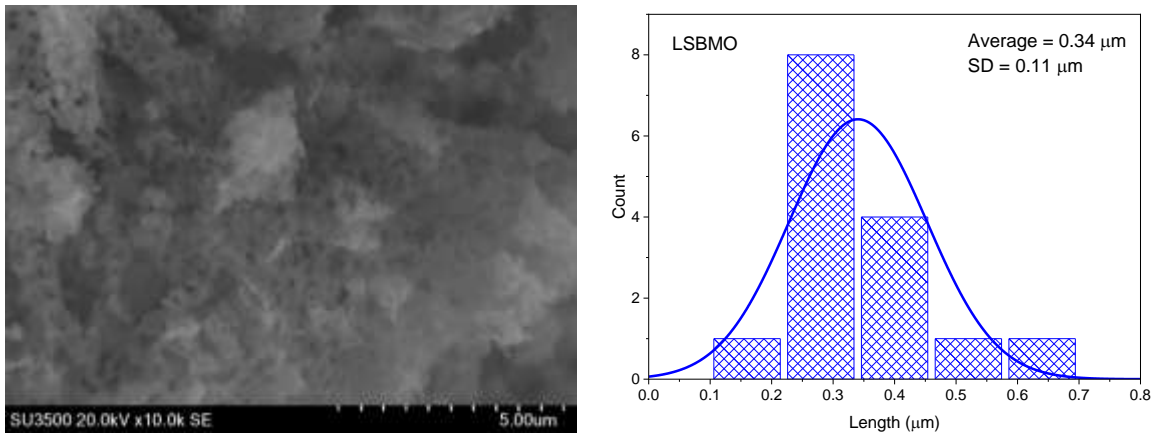
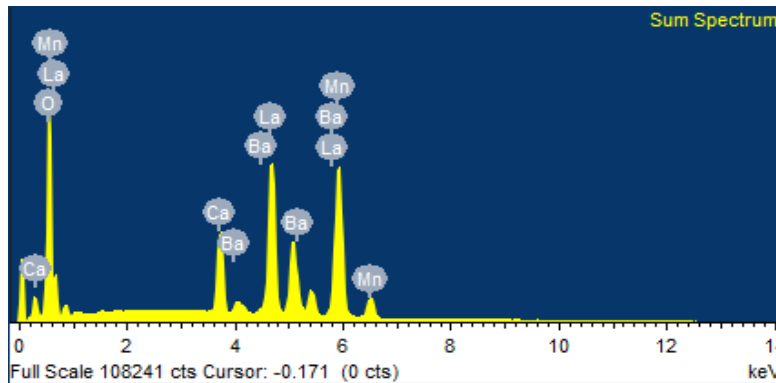
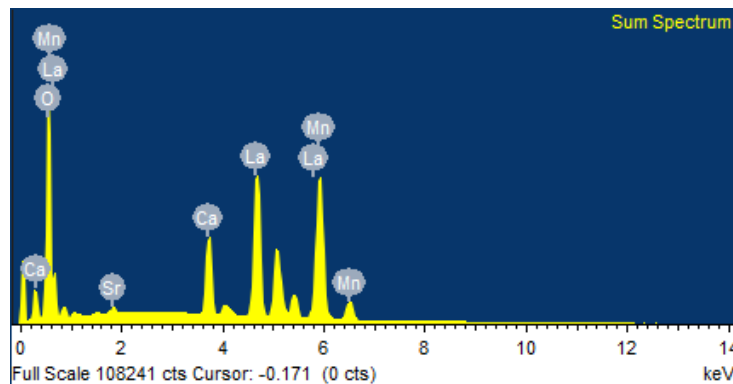


Figure 3. SEM magnified sample morphology and particle size distribution of samples (a) LCBMO, (b) LCSMO, (c) LSBMO

The LCBMO sample has an average particle size of 345 nm, the LCSMO sample is 329 nm, and the LSBMO sample is 340 nm. The histogram presented in the figure is a graph that shows the particle size distribution in each sample. In addition to SEM, the samples were also characterized using EDS to determine the composition of each element forming the sample. EDS testing is also supporting evidence that the sample does not contain other phases in the form of impurities or impurities trapped as indicated by the number of element compositions is 100%.



(a)



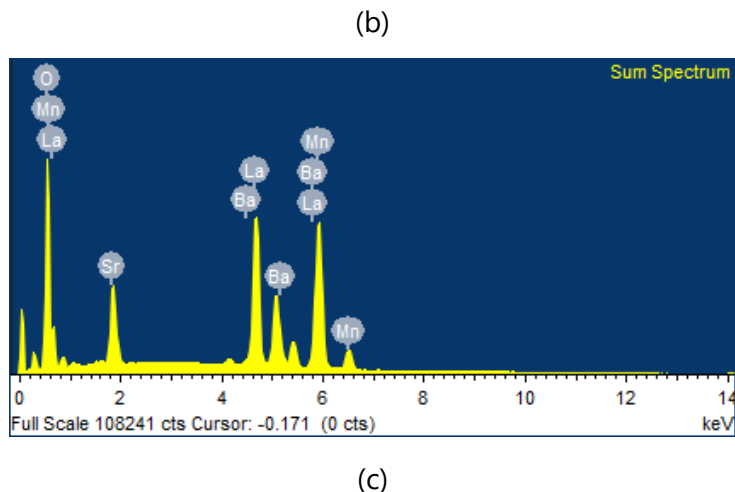


Figure 4. EDS characterization results on samples (a) LCBMO, (b) LCSMO, (c) LSBMO

The particle size of the sample has an attachment to the crystal size of the sample. This shows that the XRD and SEM test results are related. As summarized in Table 2, the particle size and crystal size of the XRD and SEM samples are slightly different. The XRD results show that the smallest crystal size belongs to the LSBMO sample while the SEM results show that the smallest particle size belongs to the LCSMO sample.

Table 2. Correlation between XRD and SEM-EDS results

| Sample | Element Weight (%) | | | | | | Particle Size (nm) | Crystallite Size (nm) |
|--------|--------------------|------|-------|------|-------|-------|--------------------|-----------------------|
| | La | Ca | Sr | Ba | Mn | O | | |
| LCBMO | 42.45 | 5.47 | - | 0.43 | 25.91 | 25.73 | 345 | 51.78 |
| LCSMO | 41.22 | 5.38 | 0.64 | - | 25.37 | 27.39 | 329 | 47.20 |
| LSBMO | 41.03 | - | 10.15 | 0.57 | 24.77 | 23.49 | 340 | 40.58 |

Magnetic Properties

Measurement of the magnetic properties of $\text{La}_{0.7}[\text{X}_{0.95}\text{Y}_{0.05}]_{0.3}\text{MnO}_3$ {XY = (Ca,Ba), (Ca,Sr), and (Sr,Ba)} samples was carried out through VSM testing using a 2 T magnetic field at room temperature. The test results can be seen in Figure 5.

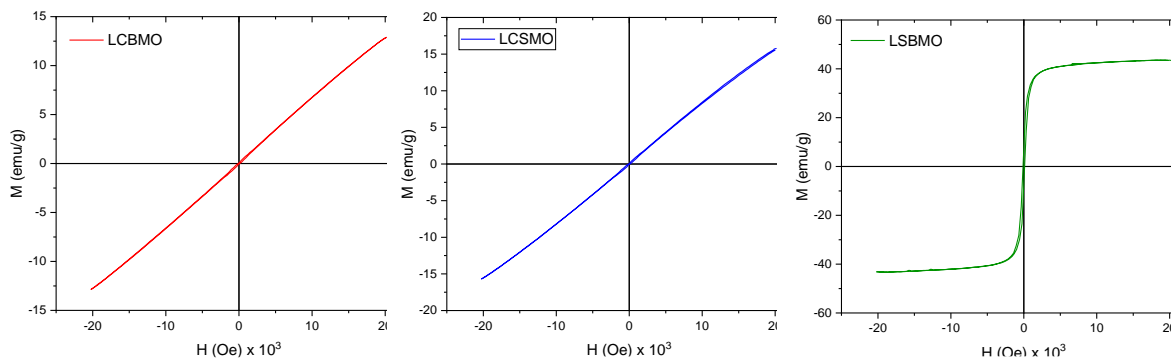


Figure 5. Magnetization graph of $\text{La}_{0.7}[\text{X}_{0.95}\text{Y}_{0.05}]_{0.3}\text{MnO}_3$ {XY = (Ca,Ba), (Ca,Sr), and (Sr,Ba)} sample against magnetic field at room temperature

In Figure 5, it can be seen that the samples have small magnetization properties characterized by the absence of hysteresis formed. LCBMO and LCSMO samples have magnetic saturation below 20 emu/g, remanent magnetization less than 0.2 emu/g, and coercivity fields of only 94.46883 Oe and 107.1359 Oe which makes these two samples paramagnetic. The LSBMO sample produces superparamagnetic properties with the provisions of magnetic saturation of 43.43736 emu/g, remanent magnetization of 0.216275 emu/g, and a high coercivity field of 14459.51 Oe. Samples with Sr and Ba substitution caused an increase in magnetization value compared to LCBMO and LCSMO samples. Full details of the VSM characterization results are in Table 3.

Table 3. VSM characterization results of $\text{La}_{0.7}[\text{X}_{0.95}\text{Y}_{0.05}]_{0.3}\text{MnO}_3$ {XY = (Ca,Ba), (Ca,Sr), and (Sr,Ba)}

| Sample | M_s (emu/g) | M_r (emu/g) | H_c (Oe) |
|--------|---------------|---------------|------------|
| LCBMO | 12.91142 | 0.187037 | 94.46883 |
| LCSMO | 15.7618 | 0.167262 | 107.1359 |
| LSBMO | 43.43736 | 0.216275 | 14459.51 |

The addition of Ca^{2+} , Ba^{2+} , dan Sr^{2+} ions on La^{3+} site causes an interaction called Double Exchange, which is the change of Mn^{3+} to Mn^{3+} and Mn^{4+} [29], [30]. However, apparently it does not have a significant effect on its magnetic properties or DE interactions that occur are weak so that the ferromagnetic magnetic regularity is also reduced.

Microwave Absorber

The VNA characterization results show the level of ability of the $\text{La}_{0.7}[\text{X}_{0.95}\text{Y}_{0.05}]_{0.3}\text{MnO}_3$ {XY = (Ca,Ba), (Ca,Sr), and (Sr,Ba)} sample in absorbing electromagnetic waves. The measured frequency values in the X-band range (8-12 GHz) and reflection loss (RL) for each sample are then connected in the form of absorption curves in Figure 6 based on the Through Power formula in Equation (3) [31].

$$\text{Through Power (\%)} = 100 \times (1 - |\Gamma|^2) \quad (3)$$

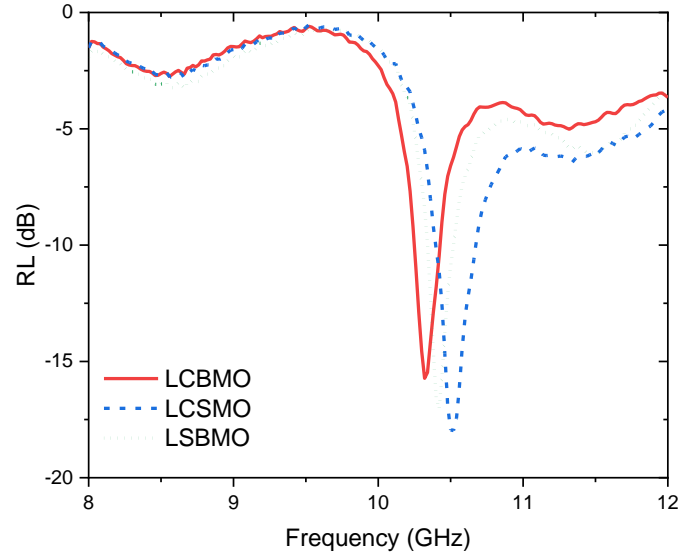


Figure 6. The absorption curve of $\text{La}_{0.7}[\text{X}_{0.95}\text{Y}_{0.05}]_{0.3}\text{MnO}_3$ {XY = (Ca,Ba), (Ca,Sr), and (Sr,Ba)}

Based on Table 4, the $\text{La}_{0.7}[\text{Ca}_{0.95}\text{Sr}_{0.05}]_{0.3}\text{MnO}_3$ or LCSMO sample has the highest microwave absorption ability at the optimum frequency of 10.5 GHz, the RL value reaches -17.94 dB. These results are also supported by the analysis of the physical properties of VNA in the form of resistance and reactance values used to obtain impedance and reflection loss. The most visible negative reflection loss value is found at a resistance of 57.71Ω and the minimum reactance is the smallest.

Table 4. VNA characterization test results of $\text{La}_{0.7}[\text{X}_{0.95}\text{Y}_{0.05}]_{0.3}\text{MnO}_3$ {XY = (Ca,Ba), (Ca,Sr), and (Sr,Ba)}

| Parameters | LCBMO | LCSMO | LSBMO |
|-------------------------|--------|--------|--------|
| Frequency (GHz) | 10.32 | 10.5 | 10.42 |
| RL (dB) | -15.76 | -17.94 | -17.04 |
| Resistance (Ω) | 45.35 | 57.71 | 44.20 |
| Reactance (Ω) | 15.09 | -11.35 | 12.03 |
| $ \Gamma $ | 0.16 | 0.13 | 0.14 |
| Through Power (%) | 97.44 | 98.31 | 98.04 |

However, this study of lanthanum manganate doped with Ca, Sr, and Ba on the La side resulted in an evenly good absorption capability, reaching 97% - 98%. However, it can be further developed based on innovative technical and methodological considerations so that these materials can have the opportunity to become real microwave absorbing functional devices.

CONCLUSION

Based on the research, it can be seen that $\text{La}_{0.7}[\text{X}_{0.95}\text{Y}_{0.05}]_{0.3}\text{MnO}_3$ (XY = (Ca,Ba), (Ca,Sr), and (Sr,Ba)) material has been successfully synthesized using sol-gel method. XRD analysis showed an orthorhombic crystal structure (Pbnm(62)). The addition of Ca^{2+} , Ba^{2+} , and Sr^{2+} ions did not change the structure but changed the lattice parameters, volume, and crystallite size. The surface morphology of the sample characterized using SEM shows that $\text{La}_{0.7}[\text{Ca}_{0.95}\text{Sr}_{0.05}]_{0.3}\text{MnO}_3$ has the smallest particle size of 329 nm. Then the EDS results state that $\text{La}_{0.7}[\text{Ca}_{0.95}\text{Ba}_{0.05}]_{0.3}\text{MnO}_3$, $\text{La}_{0.7}[\text{Ca}_{0.95}\text{Sr}_{0.05}]_{0.3}\text{MnO}_3$, and $\text{La}_{0.7}[\text{Sr}_{0.95}\text{Ba}_{0.05}]_{0.3}\text{MnO}_3$ all compositions have been evenly distributed without any trapped impurities. VSM results show that the addition of Sr^{2+} and Ba^{2+} in one formula can increase magnetization so that LSBMO has super-paramagnetic properties, while LCBMO and LCSMO are paramagnetic. The VNA test displays the effective microwave absorption capability for all three samples which managed to reach Through Power 97% - 98%, while the highest capability is owned by the LCSMO sample with RL -17.94 dB at the optimal frequency of 10.5 GHz.

ACKNOWLEDGMENT

The authors sincerely thank the Integrated Laboratory Center of UIN Syarif Hidayatullah Jakarta and the National Research and Innovation Agency for their support and willingness to help provide facilities during the research.

REFERENCES

- [1] M. Zhang *et al.*, "Multifunctional Ag-ZrB₂ composite film with low infrared emissivity, low visible light reflectance and hydrophobicity," *Applied Surface Science*, vol. 604, 2022, doi: <https://doi.org/10.1016/j.apsusc.2022.154626>.
- [2] M. F. Elmahaishi, R. S. Azis, I. Ismail, and F. D. Muhammad, "A review on electromagnetic microwave absorption properties: their materials and performance," *Journal of Materials Research and Technology*, vol. 20, pp. 2188–2220, 2022, doi: <https://doi.org/10.1016/j.mrt.2022.07.140>.
- [3] S. Sharma, S. R. Parne, S. S. S. Panda, and S. Gandi, "Progress in microwave absorbing materials: A critical review," *Advances in Colloid and Interface Science*, vol. 327, 2024, doi: <https://doi.org/10.1016/j.cis.2024.103143>.

- [4] S. Zhang *et al.*, "Two-dimensional nanomaterials for high-efficiency electromagnetic wave absorption: An overview of recent advances and prospects," *Journal of Alloys and Compounds*, vol. 893, p. 162343, 2022, doi: <https://doi.org/10.1016/j.jallcom.2021.162343>.
- [5] Y. H. Lee and R. Mahendiran, "Transport and electron spin resonance studies in Mo-doped LaMnO₃," *AIP Advances*, vol. 13(2), p. 025115, 2023, doi: <https://doi.org/10.1063/9.0000442>.
- [6] S. Moratal, R. Benavente, M. D. Salvador, F. L. Penaranda-Foix, R. Moreno, and A. Borrel, "Microwave sintering study of strontium-doped lanthanum manganite in a single-mode microwave with electric and magnetic field at 2.45 GHz," *Journal of the European Ceramic Society*, vol. 42, no. 13, pp. 5624–5630, 2022, doi: <https://doi.org/10.1016/j.jeurceramsoc.2022.05.060>.
- [7] P. Negi and A. Kumar, "MoS₂ Nanoparticle/Activated Carbon Composite as A Dual-Band Material for Absorbing Microwaves," *Royal Society of Chemistry*, vol. 3, pp. 4196–4206, 2021, doi: 10.1039/d1na002924.
- [8] F. Wang *et al.*, "Improved electromagnetic dissipation of Fe doping LaCoO₃ toward broadband microwave absorption," *Journal of Materials Science & Technology*, vol. 105, pp. 92–100, 2022, doi: <https://doi.org/10.1016/j.mst.2021.06.058>.
- [9] T. Wang, X. Qian, D. Yue, X. Yan, H. Yamashita, and Y. Zhao, "CaMnO₃ perovskite nanocrystals for efficient peroxydisulfate activation," *Chemical Engineering Journal*, vol. 398, p. 125638, 2020, doi: <https://doi.org/10.1016/j.cej.2020.125638>.
- [10] W. Deng *et al.*, "Morphology modulated defects engineering from MnO₂ supported on carbon foam toward excellent electromagnetic wave absorption," *Carbon*, vol. 206, pp. 192–200, 2023, doi: <https://doi.org/10.1016/j.carbon.2023.02.039>.
- [11] J. Zheng *et al.*, "Enhanced Electrochemical Performance of LaMnO₃ Nanoparticles by Ca/Sr Doping," *Coatings*, vol. 14, no. 20, pp. 2–9, 2023, doi: <http://dx.doi.org/10.3390/coatings14010020>.
- [12] Y. Cao *et al.*, "Recent advances in perovskite oxides as electrode materials for supercapacitors," *Chemical Communications*, vol. 57, no. 19, pp. 2343–2355, 2021, doi: <https://doi.org/10.1039/D0CC07970G>.
- [13] I. Wandira, P. K. Karo, and W. A. Adi, "Material Absorber Gelombang Elektromagnetik Berbasis (La_{0.8}Ba_{0.2}(Mn_(1-x)Zn_xFe_{(1-x)/2})O₃(x = 0–0,6)," *Jurnal Teori dan Aplikasi Fisika*, vol. 06, no. 01, pp. 63–72, 2018.
- [14] G. H. Jonker and J. H. Van Santen, "Ferromagnetic Compounds of Manganese with Perovskite Structure," *Physica*, vol. 16, no. 3, pp. 337–349, 1950, doi: [https://doi.org/10.1016/0031-8914\(50\)90033-4](https://doi.org/10.1016/0031-8914(50)90033-4).

- [15] L. Liu *et al.*, "Effects of Gd doping on microwave absorption properties and mechanism for CaMnO₃ perovskites," *Ceramics International*, vol. 49, no. 14, pp. 23499–23509, 2023, doi: <https://doi.org/10.1016/j.ceramint.2023.04.183>.
- [16] X. Zeng, X. Cheng, R. Yu, and G. D. Stucky, "Electromagnetic microwave absorption theory and recent achievements in microwave absorbers," *Carbon*, vol. 268, pp. 606–623, 2020, doi: <https://doi.org/10.1016/j.carbon.2020.07.028>.
- [17] L. Zhang, Y. Zhang, Y. D. Zhen, and S. P. Jiang, "Lanthanum Strontium Manganite Powders Synthesized by Gel-Casting for Solid Oxide Fuel Cell Cathode Materials," *Journal of the American Ceramic Society*, vol. 90, no. 5, pp. 1406–1411, 2007, doi: <https://doi.org/10.1111/j.1551-2916.2007.01568.x>.
- [18] S. Moratal, R. Benavente, M. D. Salvador, F. L. Peñaranda-Foix, R. Moreno, and A. Borrell, "Microwave sintering study of strontium-doped lanthanum manganite in a single-mode microwave with electric and magnetic field at 2.45 GHz," *Journal of the European Ceramic Society*, vol. 42, no. 13, pp. 5624–5630, 2022, doi: <https://doi.org/10.1016/j.jeurceramsoc.2022.05.060>.
- [19] G. Jayakumar, D. S. Poomagal, A. Al. Irudayaraj, A. D. Raj, S. K. Thresa, and P. Akhsadha, "Study on structural, magnetic and electrical properties of perovskite lanthanum strontium manganite nanoparticles," *Journal of Materials Science: Materials in Electronics*, vol. 31, no. 11, pp. 20945–20953, 2020, doi: 10.1007/s10854-020-04608-9.
- [20] A. Princivalle and E. Djurado, "Nanostructured LSM/YSZ composite cathodes for IT-SOFC: A comprehensive microstructural study by electrostatic spray deposition," *Solid State Ionic*, vol. 179, no. 33–34, pp. 1921–1928, 2008, doi: <https://doi.org/10.1016/j.ssi.2008.05.006>.
- [21] F. Rizky, S. A. Saptari, A. Tjahjono, and D. S. Khaerudini, "Perovskite Manganit Analysis Based on La_{0.7}Ca_{0.3}Mn_{1-x}Ti_xO₃ (x=0, 0.1, 0.2, and 0.3) as Potential Microwave Absorber Material with Sol-Gel Method," *Journal of Physics: Theories and Applications*, vol. 6, no. 1, pp. 17–24, 2022, doi: <https://dx.doi.org/10.20961/jphystheor-appl.v6i1.59142>.
- [22] R. I. Admi, S. A. Saptari, A. Tjahjono, W. A. Adi, and I. N. Rahman, "Synthesis and Characterization Microwave Absorber Properties of La_{0.7}(Ca_{1-x}Sr_x)_{0.3}MnO₃ Prepared by Sol-Gel Method," in *The 10th International Conference on Theoretical and Applied Physics (ICTAP2020) Journal of Physics: Conference Series*, IOP Publishing, 2021, pp. 1–7. doi: [doi:10.1088/1742-6596/1816/1/012091](https://doi.org/10.1088/1742-6596/1816/1/012091).
- [23] Y. Taryana, W. A. Adi, D. Mahmudin, and Y. Wahyu, "Structural, Magnetic and Microwave Absorption Characteristics of Ba_{1-x}La_xFe₂O₁₉ (x = 0; 0.1; 0.2;0.3;0.5;0.7)," *Key Engineering Materials*, vol. 855, pp. 261–267, 2020, doi: <http://dx.doi.org/10.4028/www.scientific.net/KEM.855.261>.

- [24] E. Ahilandeswari, K. Sakthipandi, R. R. Kanna, M. Hubalovska, and D. Vigneswaran, "Lanthanum substitution effect on the structural, optical, and dielectrical properties of nanocrystalline BaFe₂O₄ ferrites," *Physica B: Condensed Matter*, vol. 635, p. 413849, 2022, doi: <https://doi.org/10.1016/j.physb.2022.413849>.
- [25] L. Phor and V. Kumar, "Structural, magnetic and dielectric properties of lanthanum substituted Mn_{0.5}Zn_{0.5}Fe₂O₄," *Ceramics International*, vol. 45, no. 17, pp. 22972–22980, 2019, doi: <https://doi.org/10.1016/j.ceramint.2019.07.341>.
- [26] B. H. Toby, "EXPGUI, a graphical user interface for GSAS," *Journal of Applied Crystallography*, vol. 34, no. 2, pp. 210–213, 2004, doi: <https://doi.org/10.1107/S0021889801002242>.
- [27] R. Hamdi, S. S. Hayek, A. M. Samara, Y. Tong, S. A. Mansour, and Y. S. Haik, "Williamson-Hall technique for magnetic cooling in nanosized manganite LaNi_{0.25}Mn_{0.75}O₃ and ferrite LaNi_{0.25}Fe_{0.75}O₃," *Solid State Sciences*, vol. 142, p. 107223, 2023, doi: <https://doi.org/10.1016/j.solidstatesciences.2023.107223>.
- [28] P. Orgiani *et al.*, "Multiple double-exchange mechanism by Mn²⁺ doping in manganite compounds," *Physical Review B*, vol. 82, no. 20, p. 205122, 2010, doi: <https://doi.org/10.1103/PhysRevB.82.205122>.
- [29] E. Pavarini and E. Koch, "Origin of Jahn-Teller distortion and orbital-order in LaMnO₃," *Physical Review Letters*, vol. 104, no. 8, p. 086402, 2010, doi: https://doi.org/10.1103/PhysRevLett.104.086402?_gl=1*16ig9nd*_gcl_au*NTlxNDc4NDQ5LjE3MzI2OTEzODg.*_ga*OTQxNDY5MDQ3LjE3MzI2OTEzODU.*_ga_ZS5V2B2DR1*MTczMjY5MTM4OC4xLjAuMTczMjY5MTM4OC42MC4wLjlxMDc0Mjk0NzM.
- [30] H. Cheng, H. Chen, C. Jin, and H. Bai, "Modulating the antiferromagnetic metallic and insulating states by lattice distortion for lightly-doped La_{0.92}Sr_{0.08}MnO₃ films," *Journal of Magnetism and Magnetic Materials*, vol. 565, p. 170300, 2023, doi: <https://doi.org/10.1016/j.jmmm.2022.170300>.
- [31] W. A. Adi *et al.*, *Electromagnetic Fields and Waves, Metamaterial: Smart magnetic Material for Microwave Absorbing Material*. United Kingdom: IntechOpen, 2019. doi: [10.5772/intechopen.84471](https://doi.org/10.5772/intechopen.84471).